Depth-Dependent Hemoglobin Analysis From Multispectral Transillumination Images

Brian D'Alessandro* and Atam P. Dhawan

***Abstract*—Multispectral transillumination imaging is a promising modality for noninvasive imaging of living tissue. Multispectral Nevoscope imaging is directed toward the imaging of skin lesions for the detection and characterization of skin cancers through the volumetric analysis of selected chromophores, such as melanin, oxy-, and deoxyhemoglobin. In this letter, we present a novel method of recovering depth-dependent measurements from transillumination images obtained through the Nevoscope. A method for estimating the depth-dependent point spread function is presented and used in recovering multispectral transillumination images of a skin phantom or lesion through blind deconvolution. A method for ratiometric analysis for the quantification of oxy- and deoxyhemoglobin is then presented and evaluated on a skin phantom. The presented methods would allow reliable quantitative analysis of multispectral Nevoscope images for early detection of angiogenesis leading to early diagnosis of skin cancers.**

***Index Terms*—Biomedical optical imaging, deconvolution, diffuse reflectance imaging, transillumination.**

I. Introduction

SKIN cancer is a common form of malignancy. While malignant melanoma is the deadliest form of skin cancer, the survival rate is excellent if it is detected and diagnosed early. Noninvasive optical imaging techniques have been investigated to image skin lesions for mass screening to detect and analyze the morphological changes associated with tumorigenesis, thereby improving patient diagnosis accuracy. Deeper subsurface information, such as subcutaneous pigmentation and increased blood flow (angiogenesis) are critical factors in early melanoma detection.

II. Procedures and Methods

One optical imaging modality currently being investigated to obtain critical subsurface information is transillumination. An optical instrument, the Nevoscope, has been developed for transillumination light microscopy for imaging skin lesions [1]. The Nevoscope uses a fiber-optic illumination ring to transmit light directly into the skin at an angle so that the light is diffused across the layers of skin behind the lesion. The backscattered light photon energy forms a transilluminated image of the skin and skin lesion [see Fig. 1(a)].

Manuscript received April 22, 2010; revised June 16, 2010; accepted July 9, 2010. Date of publication July 15, 2010; date of current version September 15, 2010. *Asterisk indicates corresponding author.*

*B. D'Alessandro is with the Department of Electrical and Computer Engineering, New Jersey Institute of Technology, Newark, NJ 07102 USA (e-mail: bmd5@njit.edu).

A. P. Dhawan is with the Department of Electrical and Computer Engineering, New Jersey Institute of Technology, Newark, NJ 07102 USA (e-mail: dhawan@njit.edu).

Color versions of one or more of the figures in this paper are available online at http://ieeexplore.ieee.org.

Digital Object Identifier 10.1109/TBME.2010.2059025

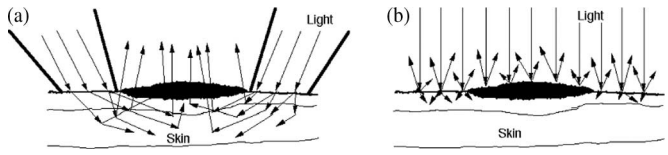

Fig. 1. (a) Transillumination and (b) surface reflectance imaging.

Because of the geometry of the Nevoscope and the angle at which light enters the skin, it provides an excellent method of imaging deeper skin structures. In addition, longer wavelengths of light penetrate deeper in the skin than shorter wavelengths. Consequently, multispectral transillumination imaging provides a way to obtain depth-resolved information on subsurface skin features, such as blood volume. Multispectral imaging of skin lesions with the Nevoscope has been used for the enhanced detection of malignant melanomas [2]. However, estimating specific information about depth of structures and chromophores, such as oxygenated hemoglobin (HbO_2) and deoxygenated hemoglobin (Hb) in the lesion from transillumination or diffuse reflectance images is a challenging task. If such an estimation could reliably be done, it would open up far reaching applications in tissue characterization and angiogenesis analysis, including neural imaging.

The diffuse reflectance measurements emerging from different depths in the tissue pose a challenge in image restoration for reliable quantitative analysis, as the point spread function (PSF) is both wavelength and depth dependent. In this letter, a novel method for determining this depth and wavelength-dependent PSF is presented and then used to restore multispectral transillumination images obtained with the Nevoscope. Images are then quantitatively analyzed for determination of the volumetric distribution of selected chromophores, such as Hb and HbO_2 to investigate angiogenesis in the skin lesion for early diagnosis and characterization of skin cancers. The method is evaluated using a skin phantom with artificial Hb or HbO_2 distributed through capillary tubes in a medium with spectral characteristics similar to human skin.

III. Skin Phantom

To develop and evaluate a method for determining the depth-dependent PSF for multispectral transillumination imaging, a tissue-like skin phantom was built in a dish container with embedded capillaries to be filled with artificial Hb, HbO_2, or any other material as needed. The phantom base material consisted of Al_2O_3 particles, cosmetic powder, and silicone, matching the spectral properties of skin for the visible and near-infrared range [3]. Before curing the phantom, five capillary tubes were embedded at equally spaced depths [see Fig. 2(a)]. Each tube is 1 mm in diameter and is positioned at depths in increments of 0.5 mm [see Fig. 2(b)], spanning the typical thickness range of a skin

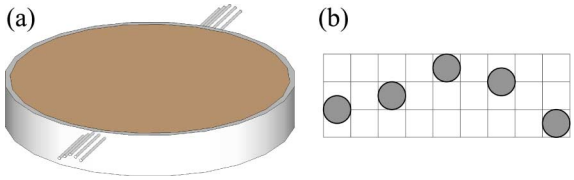

Fig. 2. (a) Phantom with capillary tubes. (b) Tube layout (1 mm × 1 mm grid).

lesion. The tubes were filled with either red or blue food coloring to simulate the presence of subsurface HbO_2 and Hb, which were found to approximate the wavelength-dependant absorption differences of real HbO_2 and Hb. The phantom was transilluminated by the Nevoscope at 600-, 680-, 780-, 800-, or 875-nm wavelengths for multispectral imaging. The backscattered diffuse-reflectance-based images from the skin phantom were recorded using a multispectral Andor Luca CCD camera with 1000 × 1000 pixel resolution. Images were normalized to correct for the exposure time as well as the relative response curve of the light source and CCD. Images with empty tubes were used to normalize with respect to the background.

IV. PSF Estimation and Deconvolution

The impulse response of a camera's optical system is known as the PSF. The image of a structure deep within the skin tissue is degraded or blurred due to scattering effects and light diffusion. Blurring increases the deeper a structure is. Thus, a point structure at different depths produces different PSFs, and the deeper the point, the more spread out the PSF should be. If f is the ideal, depth-resolved image with full structure clarity and h is the PSF, then the degraded image g is defined as the convolution of f and h in terms of pixel location (i, j) by the following:

$$g(i,j) = f(i,j) \otimes h(i,j) \tag{1}$$

where $\otimes$ is the convolution operator. To find f, given g and h, the opposite process of deconvolution must be used. Since noise is also present in any real-world system, only an estimate of f can be found, or $\hat{f}$. One method of doing this is to employ the Weiner deconvolution filter in the frequency domain. If G, F, and H are the Fourier transforms of g, f, and h, respectively, and (u, v) is the Fourier transform coefficient locations, the Weiner deconvolution filter is defined by the following:

$$\hat{F}(u,v) = \left[\frac{H^*(u,v)}{|H(u,v)|^2 + 1/\mathrm{SNR}}\right] G(u,v) \tag{2}$$

where SNR is the signal-to-noise ratio. The inverse Fourier transform of $\hat{F}$ provides an estimate of the true image [4].

Of course, the exact PSF and SNR are not always known, and consequently, must be modeled. The structure in the skin phantom at each depth level is a straight tube; therefore, its respective edge spread function, rotated radially, is used as the initial PSF guess in an iterative Lucy–Richardson maximum likelihood blind deconvolution algorithm operating on the diffused reflectance image with noise effects smoothed out. For the kth iteration, the next estimate of the deconvolved image and PSF are expressed as follows:

$$\hat{f}_{k+1} = \hat{f}_k \left(h_k * \frac{g}{\hat{f}_k \otimes h_k}\right)$$
$$h_{k+1} = h_k \left(\hat{f}_k * \frac{g}{\hat{f}_k \otimes h_k}\right) \tag{3}$$

where $*$ is the correlation operator [5]. After ten iterations of the blind deconvolution algorithm, the PSF converges. Since the tube is positioned vertically, the horizontal cross section is extracted and rotated about its center to produce a circularly symmetric PSF. The result is an improved PSF, which is a better estimate of the imaging impulse response at a given tissue depth and transillumination wavelength. The PSF h with an estimated SNR of 17.0 dB is then used in Weiner filtering.

V. Multichromophore Measurement

While depth-dependant deconvolution is important, total absorption images must be separated into individual chromophore contributions. Diffusion theory has been used as an approximation of the radiative transport equations to describe light propagation in a turbid medium. Solutions to the diffusion equation generally show an exponential attenuation of light in a medium for a given depth, with the wavelength-dependent absorption and scattering coefficients as $\mu_a(\lambda)$ and $\mu_s(\lambda)$. To simplify, the minimum penetration depth level is assumed among all selected wavelengths for ratiometric analysis, and μ_s is assumed to be constant over the selected spectral bandwidth. Considering these constraints, for a specific wavelength λ, the diffused light remittance intensity A_λ at a particular point is roughly proportional to $\mu_a(\lambda)$ and can be considered as the grey-level value of an imaged pixel. Although the spatial dependence of the absorption coefficients cannot be *exactly* known, A_λ is related to the absorption of each chromophore present in the medium. These absorptions are assumed to be linearly combined for imaging. Since the major chromophores in the skin are melanin, HbO_2, and Hb, the total normalized absorption is a function of the unknown amount of melanin [Mel], oxyhemoglobin [HbO_2], and deoxyhemoglobin [Hb]

$$A_\lambda = [\mathrm{Mel}]\,\mu^\lambda_{\mathrm{Mel}} + [\mathrm{HbO_2}]\,\mu^\lambda_{\mathrm{HbO_2}} + [\mathrm{Hb}]\,\mu^\lambda_{\mathrm{Hb}} \tag{4}$$

where $\mu^\lambda_{\mathrm{Mel}}$, $\mu^\lambda_{\mathrm{HbO_2}}$, and $\mu^\lambda_{\mathrm{Hb}}$ are the wavelength-dependent absorption coefficients of melanin, HbO_2, and Hb, respectively.

With three unknowns, three equations, or three imaging wavelengths are needed to estimate the amounts of each chromophore. Given the imaged pixel values for 680-, 780-, and 800-nm images, as well as the absorption coefficients of melanin, HbO_2, and Hb, a linear system can be used to estimate [Mel], [HbO_2], and [Hb] present under the area imaged by the pixel. To find an estimate of the *total* relative absorption for Hb and HbO_2 across the 100 nm between 680 nm and 780 nm, we compute a linear approximation of the area underneath the absorption curve for each chromophore, modified by the amount of that chromophore as follows:

$$\overline{\mathrm{Hb}} = 0.5([\mathrm{Hb}]\mu^{680}_{\mathrm{Hb}} + [\mathrm{Hb}]\mu^{780}_{\mathrm{Hb}})(100\ \mathrm{nm}) \tag{5}$$
$$\overline{\mathrm{HbO_2}} = 0.5([\mathrm{HbO_2}]\mu^{680}_{\mathrm{HbO_2}} + [\mathrm{HbO_2}]\mu^{780}_{\mathrm{HbO_2}})(100\ \mathrm{nm}). \tag{6}$$

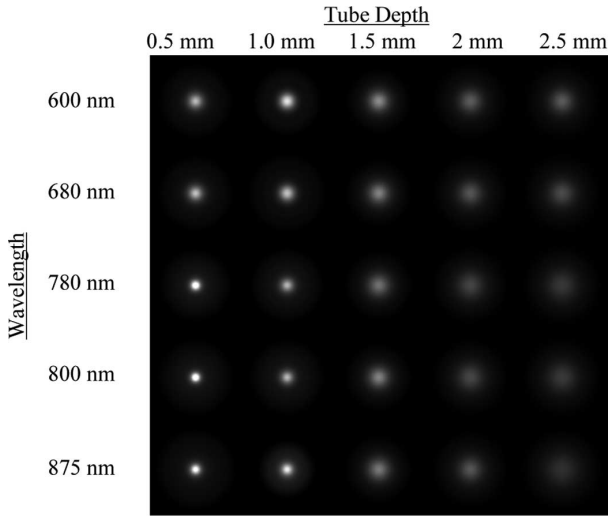

Fig. 3. PSF estimates: wavelength versus depth.

The $\overline{\text{HbO}_2}$ estimate itself relates to how much spectral absorption is caused by HbO_2, and therefore, is a measure of blood oxygen saturation (SO_2). Thus, if we want to visualize SO_2 and its spatial localization, we can simply analyze the $\overline{\text{HbO}_2}$ image. Another method of visualization is to compute a ratiometric measurement defining SO_2 relative to the total amount of blood. Total blood is simply $\overline{\text{HbO}_2} + \overline{\text{Hb}}$; therefore, our normalized ratiometric measurement of percent oxygen saturation in the blood is the following:

$$R = \frac{\overline{\text{HbO}_2}}{\overline{\text{HbO}_2} + \overline{\text{Hb}}}. \tag{7}$$

All of the aforementioned equations are evaluated pixel by pixel, resulting in 2-D solutions for $\overline{\text{HbO}_2}$, $\overline{\text{Hb}}$, and R.

No melanin is present in the skin phantom, thus imaging at only two wavelengths is needed (680 and 780 nm) to solve for [HbO_2] and [Hb]. Two tubes (0.5 and 1.0 mm) are filled first with artificial HbO_2 and then with artificial Hb. Each set of images is deconvolved with the 0.5-mm PSF for the respective wavelength using the procedure mentioned earlier. The multispectral set of images are then evaluated using (4)–(7), and results for the HbO_2 and Hb area estimates are shown in Fig. 6.

VI. Results and Discussion

The blind deconvolution process was repeated for each of the five tube depths and each of the five wavelengths, producing a total of 25 PSF estimates (see Fig. 3). As expected, the PSFs for the 2.5-mm-depth are more spread out than those at 0.5 mm, since images of deeper tubes are more blurred.

Given the estimated PSFs, the next step was to observe how well they deconvolve an image of a single chromophore-filled tube. The SNR of the image acquisition was estimated by comparing a noiseless image estimate with the actual noisy image. Then, $\hat{f}(i,j)$ was found using (2) and the inverse Fourier transform. The original blurred diffuse reflectance images $g(i,j)$ as well as $\hat{f}(i,j)$ are shown in Fig. 5 for five different tube depths at 780 nm.

In each of the 25 cases, deconvolution using the estimated PSF and SNR were able to restore the tube structure to make it more recognizable than in the original image. Performance worsens

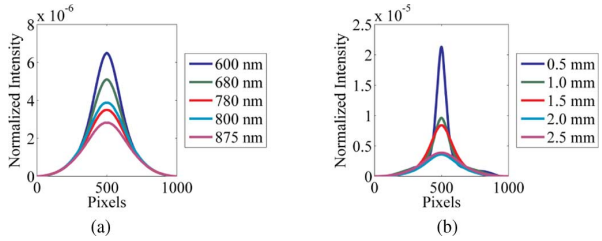

Fig. 4. PSF cross sections for 2.5-mm-deep tube and 780-nm transillumination. (a) PSF cross sections of 2.5-mm-deep tube for varying wavelengths (see 5th column of Fig. 3). (b) PSF cross sections of 780-nm transillumination for varying tube depth (see third row of Fig. 3).

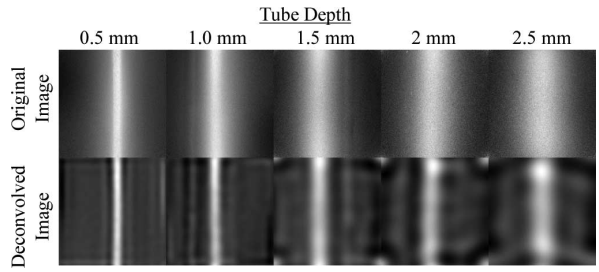

Fig. 5. Original and deconvolved images at 780 nm, for the five different tube depths. Similar results were found for 600, 680, 800, and 875 nm. Brighter pixel values (i.e., white) represent areas of high absorption.

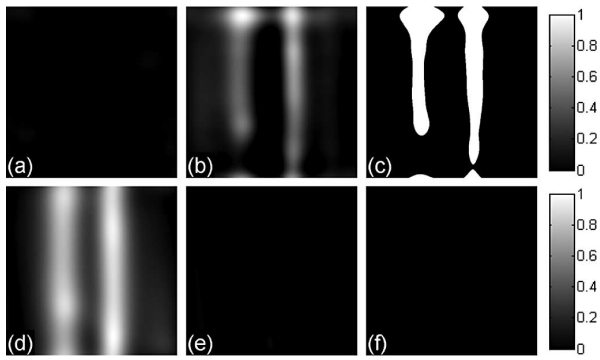

Fig. 6. For the HbO_2-filled phantom: (a) $\overline{\text{Hb}}$, (b) $\overline{\text{HbO}_2}$, and (c) R. For the Hb-filled phantom: (d) $\overline{\text{Hb}}$, (e) $\overline{\text{HbO}_2}$, and (f) R.

with increased depth; however, the general shape of deep structures can be recovered with a reasonable contrast to improve upon the diffuse reflectance image.

Interestingly, the PSFs of the skin-tissue phantom were found to vary smoothly with depth and wavelength (see Fig. 4). With this observation, curve fitting was used to find a cross-section-shape model, which fit the observed data. With this model, the PSF can be obtained for any continuous depth or wavelength value in a reasonable range; not just the specific values used in the phantom study. In general, the PSF shapes very accurately matched the sum of two Gaussian distributions. The parameters of these distributions were modeled, in terms of depth d and wavelength λ, to produce the final PSF equation in terms of d, λ, and pixel value x as follows:

$$a_1(d,\lambda) = 5.62 - 1.19d + 0.015\lambda + 2.11d^2 - 0.013d\lambda$$

$$a_2(d,\lambda) = 5.61 - 1.40d - 0.00025\lambda$$

$$c_1(d,\lambda) = 106.3 + 6.56d - 0.11\lambda - 3.77d^2 + 0.066d\lambda$$

$$c_2(d) = 140 + 40d$$

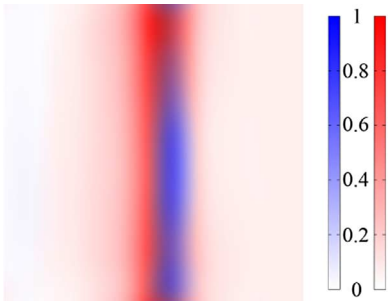

Fig. 7. $\overline{\text{Hb}}$ (blue) and $\overline{\text{HbO}_2}$ (red) overlaid for a single tube filled with 50% Hb and 50% HbO_2.

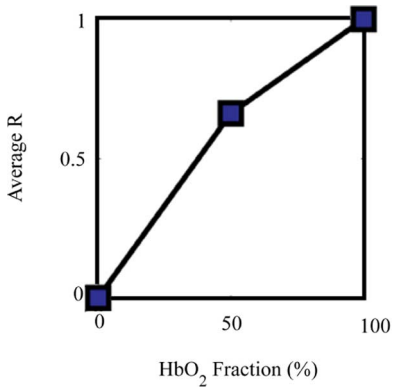

Fig. 8. Average R value in ROI for varying fractions of HbO_2 in a tube.

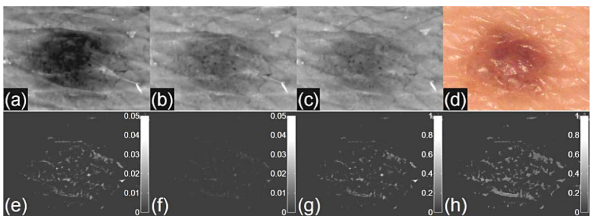

Fig. 9. Transilluminated benign skin lesion images at (a) 680 nm, (b) 780 nm, and (c) 800 nm. (d) Color surface reflectance image. (e) $\overline{\text{Hb}}$ estimate. (f) $\overline{\text{HbO}_2}$ estimate. (g) Melanin estimate. (h) Ratiometric image R.

$$\text{PSF}(x;d,\lambda) = a_1(d,\lambda)\cdot\exp\left(-\left(\frac{x}{c_1(d,\lambda)}\right)^2\right) + a_2(d,\lambda)\cdot\exp\left(-\left(\frac{x}{c_2(d)}\right)^2\right). \quad (8)$$

This equation (after normalization to ensure the sum of the area under the PDF equals 1) resulted in an R^2 coefficient of determination greater than 0.95 for all observed data, while the average R^2 was 0.987, indicating the model fits the observations very well.

Likewise, the proposed method for chromophore separation very nicely differentiates the two; for the HbO_2-filled phantom, the average $\overline{\text{Hb}}$ value is 2.2×10^{-3} [see Fig. 6(a)], while the average $\overline{\text{HbO}_2}$ value is 0.18 [see Fig. 6(b)] and clearly highlights the spatial location of HbO_2 within the two tubes. Similarly, for the Hb-filled phantom, the average $\overline{\text{HbO}_2}$ value is 2.4×10^{-4} [see Fig. 6(e)], while the average $\overline{\text{Hb}}$ value is 0.37 [see Fig. 6(d)]. The ratiometric calculation is performed on the pixels within a thresholded region of interest (ROI), defined as any pixel, where $\overline{\text{Hb}}+\overline{\text{HbO}_2}>0.4$ so as to reduce the effects of light scattering blur. In practice, the ROI is placed in the center around the skin lesion to avoid light leakage from the transillumination ring. Within this ROI for the HbO_2-filled phantom, the ratiometric values in R equal 1.0, correctly indicating that 100% of the artificial blood in that case is HbO_2 [see Fig. 6(c)]. When this R is compared with the actual tube area, the ratiometric image has an accuracy of 74.9%, which is decent considering the original complications of diffuse light scattering. On the other hand, 0% of the Hb-filled phantom is HbO_2, correctly resulting in values of zero throughout the R image [see Fig. 6(f)]. Furthermore, an experiment was performed on a single 0.5-mm-deep tube filled with a mixture of 50% Hb and 50% HbO_2 to show their separation in the mixture. Both $\overline{\text{Hb}}$ and $\overline{\text{HbO}_2}$ were successfully detected, as the overlay shows in Fig. 7. The average R value within the ROI was found to be 66.2%, and is plotted in Fig. 8 along with the average R value for 0% and 100% HbO_2. While not perfectly linear, a reasonable estimate of HbO_2 fraction can be obtained through R-value analysis.

The method was also tested on the multispectral images of a benign skin lesion using three wavelengths (see Fig. 9). The estimates of melanin, Hb, HbO_2, and R value are shown. The blood volume and ratio measurements are expected to change significantly in cancerous lesions for which validation is ongoing through clinical studies.

VII. Conclusion

In this letter, we have presented a novel depth-dependent ratiometric analysis method that can be used to quantify depth-dependent absorptions of Hb and HbO_2 for angiogenesis analysis. A wavelength and depth-dependent PSF for a specific transillumination imaging geometry, such as with the Nevoscope, can be estimated and used to deconvolve multispectral images for image restoration and subsequent ratiometric measurements of Hb, HbO_2, and relative oxygen saturation. The presented methodology can provide real-time estimation of relative depth-dependent parameters. The estimated PSFs and chromophore distributions could be used with a Monte Carlo simulation-based model for a better depth-dependent volumetric reconstruction of melanin, Hb, HbO_2, and oxygen saturation. Given the continuous nature of PSFs versus depth, it is reasonable that the depth of chromophore information may be estimated through optimization techniques, such as the genetic algorithm. Such techniques are currently being investigated. The potential impact of these methods is far reaching, not only for the characterization of skin lesions to facilitate early detection of skin cancers, but also for other applications of tissue characterization such as neural imaging.

References

[1] A. P. Dhawan, "Apparatus and method for skin lesion examination," U.S. Patent 5 146 923, Sep. 15, 1992.

[2] A. P. Dhawan, B. D'Alessandro, S. Patwardhan, and N. Mullani, "Multispectral optical imaging of skin-lesions for detection of malignant melanomas," in *Proc. IEEE Eng. Med. Biol. Soc. Conf.*, 2009, pp. 5352–5355.

[3] M. Lualdi, A. Colombo, B. Farina, S. Tomatis, and R. Marchesini, "A phantom with tissue-like optical properties in the visible and near infrared for use in photomedicine," *Lasers Surg. Med.*, vol. 28, pp. 237–243, 2001.

[4] R. C. Gonzalez and W. E. Richard, *Digital Image Processing*, 3rd ed. Upper Saddle River, NJ: Pearson Prentice Hall, 2008.

[5] T. J. Holmes, D. Biggs, and A. Abu-Tarif, "Blind deconvolution," in *Handbook of Biological Confocal Microscopy*, J. B. Pawley, Ed., 3rd ed. New York: Springer-Verlag, 2006.